In this way, from (24) the values of $P_k(s_k)$ at M discrete points can be easily obtained. We use (25a,b) and the following Chebyshev rule

$$\int_{-a}^{a} \frac{F(t)\,dt}{(a^2 - t^2)^{1/2}} \approx \frac{\pi}{M} \sum_{m=1}^{M} F(t_m), \quad t_m = a \cos \frac{(2m - 1)\pi}{2M} \tag{27}$$

The SIF values at all the crack tips can be also obtained.

In the condition of $M = 9$, the calculated numerical results are plotted in Figs. 3, 4 and 5. In the three figures, we express the SIF values as follows

$$\begin{aligned} K_{3,A} &= -F_{3A}\tau(\pi a)^{1/2}, \\ K_{3,B} &= F_{3B}\tau(\pi a)^{1/2}, \\ K_{3,C} &= -F_{3C}\tau(\pi a)^{1/2}, \\ K_{3,D} &= F_{3D}\tau(\pi a)^{1/2}. \end{aligned} \tag{28}$$

where A, B, C and D represent the four crack tips of two cracks, τ is the remote stress applied, and a is the half length of crack.

The results shown in the Fig. 3 and Fig. 4 were first obtained in this paper. In addition, the results for inner crack tip shown in the Fig. 5 coincided with those cited in Ref.[6], so the accuracy of our approach is examined by this numerical example.

REFERENCES

[1] V. V. Panasyuk, P. Savruk and A. P. Datsyshyn, A general method of solution of two-dimensional problems in the theory of cracks, *Engng Fracture Mech.*, **9**, 481–497 (1977).

[2] F. Erdogan, Mixed boundary-value problems in mechanics, *Mechanics Today* **4**, Pergamon Press, New York, 1978.

[3] P. S. Theocaris, and N. I. Ioakimidis, Numerical integration methods for the solution of singular integral equations, *Quartly Appl. Maths.* **35**, 173–183 (1977).

[4] Y. Z. Chen, A Fredholm integral equation approach for multiple crack problems in an infinite plate, *Engng Fracture Mech.* (In press) (1983).

[5] Y. Z. Chen Reducing crack problem of a circular plate or an infinite plate containing a circular hole into Fredholm integral equation, *Int. J. Fracture* **23**, R 101–104 (1983).

[6] M. Isida, Method of Laurant series expansion for internal crack problems, Mechanics of Fracture I (Methods of Analysis and Solutions of Crack Problems), (Edited by G. C. Sih,), Noordhoff Int, New York (1973).

[7] N. I. Muskhelishvili, *Some Basic Problems of Mathematical Theory of Elasticity*. Groningen, Netherlands, 1953.

(*Received* 21 *December* 1983)

Engineering Fracture Mechanics Vol. 21, No. 3, pp. 479–494, 1985
Printed in the U.S.A.

0013-7944/85 $3.00 + .00

ANALYTICAL ESTIMATION OF STRESS INTENSITY FACTORS IN PATCHED CRACKED PLATES

RAMESH CHANDRA and M. V. V. MURTHY
Structures Division, NAL, Bangalore, India

and

T. S. RAMAMURTHY and A. K. RAO
Aero. Engng Dept., IISc, Bangalore, India

Abstract—The fatigue and fracture performance of a cracked plate can be substantially improved by providing patches as reinforcements. The effectiveness of the patches is related to the reduction they cause in the stress intensity factor (SIF) of the crack. So, for reliable design, one needs an accurate evaluation of the SIF in terms of the crack, patch and adhesive parameters. In this investigation, a centrally cracked large plate with a pair of symmetric bonded narrow patches, oriented normally to the crack line, is analysed by a continuum approach. The narrow patches are treated as transversely flexible line members. The formulation leads to an integral equation which is solved numerically using point collocation. The convergence is rapid. It is found that substantial reductions in SIF are possible with practicable patch dimensions and locations. The patch is more effective when placed on the crack than ahead of the crack. The present analysis indicates that a little distance inwards of the crack tip, not the crack tip itself, is the ideal location, for the patch.

NOTATION

$2a$	crack length
$2b$	width of cracked plate or sheet
E	Young's modulus
G	shear modulus
Im	imaginary part of complex function
K_r	stress intensity factor of cracked sheet due to shear stress distribution acting between patch and sheet
K	stress intensity factor of cracked sheet with patch, subjected to uniform tensile load
$2l$	length of patch
Re	real part of complex function
t	thickness
v	displacement in y-direction
w	width of patch
z	$x + \mathrm{i}\,y$
z_0	$x_0 + \mathrm{i}\,y_0$
α	$E_p t_p w / E_s t_s a$
σ	applied uniform stress
ν	Poisson's ratio.

Subscripts

a	adhesive
p	patch
s	sheet.

INTRODUCTION

THE 'FAIL SAFE' concept is widely used in the design of aircraft structural components. Th design of such 'damage tolerant' structures is governed by detailed specifications [1, 2], whic are intended to ensure that a specified fatigue crack will not grow to critical proportions in period between successive routine inspections.

Fatigue cracked components are often repaired in service. Standard repair schemes normall involve strengthening the component by connecting a reinforcing member by means of bol or rivets and thereby reducing the crack tip stress intensity factors.

Recent technological advances in fibre reinforced composite materials and adhesive bondin have led to the development of efficient repair schemes using these. In such repairs, (a) th load transfer between component and reinforcement is affected with minimal stress concer tration effects, (b) the properties and geometry of the reinforcement can be tailored to suit th

particular application and (c) the composite repair patch does not add significantly to the weight of the component. Boron–epoxy, boron–aluminum and carbon–epoxy have been used in some repair schemes for aircraft structures [3, 4].

An efficient design of the reinforcement (patch) needs estimation of the resulting stress intensity factor (SIF) at the crack tip in the patched panel.

There have been numerous attempts [5–8] to compute SIF of patched cracked plates. These are based on the finite element technique using special elements with displacement [9] or hybrid formulation [10].

In this investigation, stress intensity factors in a large plate with a central crack, symmetrically reinforced with patches on both sides, are estimated using a continuum approach. The reinforcement is represented as a transversely flexible line member. Hence, the problem is reduced to one of a cracked plate with distributed applied shears, unknown *ab initio*. This shear force distribution is determined as follows: the displacement field in the cracked plate, due to combination of external uniaxial tensile loading and distributed shear forces caused by the patches, is obtained from elasticity solutions. The one-dimensional displacement fields in the reinforcements are directly evaluated in terms of the shear forces. Also, the differences between displacements in the sheet and patch are accounted for by the shear flexibility of the adhesive. Thus an integral equation in shear stress results. This equation is numerically solved by assuming a polynomial distribution in shear stress and employing a point collocation technique. The SIF in the cracked plate due to the distributed shear forces is then computed by using point load solutions (SIF in centrally cracked infinite plate due to two symmetric pairs of equal and opposite unit point forces). The total SIF in the patched plate is computed by the direct addition of the SIF's due to the external loading and the distributed shear forces.

2. MATHEMATICAL DEVELOPMENT

Figure 1(a) shows the configuration of a central crack in a large plate [$(b/a) > 10$], patched symmetrically. In Fig. 1(b) the patches are replaced by unknown shear stress distributions along the patch central lines. The stress intensity factor for the patched and loaded plate, Fig. 1(b) is given as

$$K = \sigma\sqrt{(\pi a)} + K_r \tag{1}$$

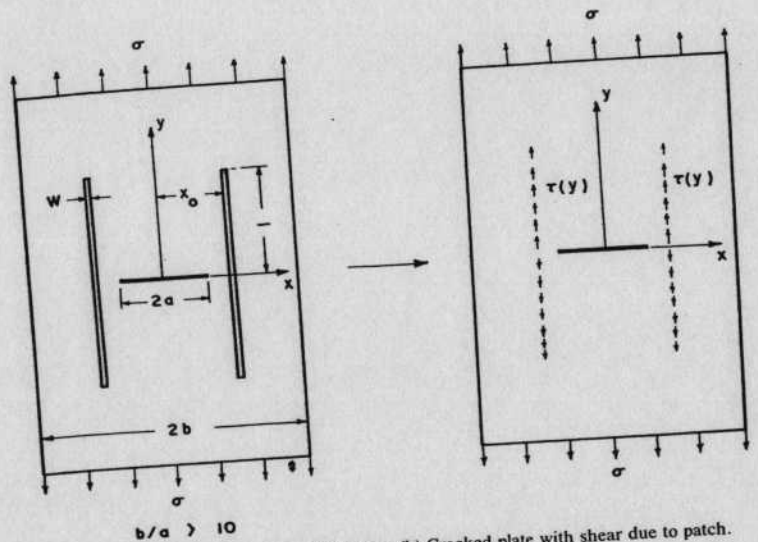

Fig. 1. (a) Configuration of patched plate. (b) Cracked plate with shear due to patch.

where

$$K_r = w \int_0^t \tau(x_0, y_0)\phi(x_0, y_0)\, dy_0$$

$\tau(x_0, y_0)$ is the shear stress at point (x_0, y_0) in the sheet and $\phi(x_0, y_0)$ is the stress intensity factor in the sheet due to the set of four unit forces acting at $(\pm x_0, \pm y_0)$. $\phi(x_0, y_0)$ was derived by Sneddon and Tweed [11] employing Fourier transforms and the results were obtained in the form of integrals, which are not convenient for the present purpose. Hence ϕ is now rederived in closed form using complex potentials (see Appendix A)

$$\phi(x_0, y_0) = -\frac{2}{t_s}\sqrt{\left(\frac{a}{\pi}\right)}\left[\text{Im}\{(z_0^2 - a^2)^{-0.5}\} - \frac{1+\nu}{2} y_0 \,\text{Re}\{z_0(z_0^2 - a^2)^{-1.5}\}\right]. \tag{2}$$

Figure 2 shows the comparison of the results of the two techniques.

2.1 *Shear stress estimation*

Under the assumption of uniform direct stresses across the thicknesses of sheet and patch, the shear stress in the adhesive is given by the formula

$$\tau = \frac{G_a}{t_a}(v_p - v_s). \tag{3}$$

Considering that the load transfer between patch and sheet is by surface shears at the interfaces with the adhesive and the other faces are shear free, it is closer to reality to model a linear distribution of shear from zero at its free surface (or mid surface in a symmetric reinforcement) to a maximum at the adhesive interface as in Fig. 3 [6]. This yields the following expression

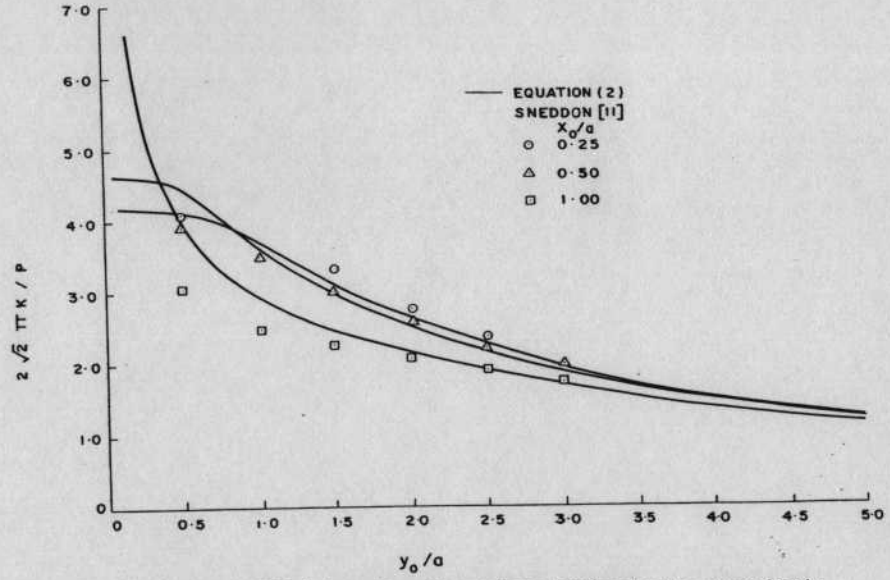

Fig. 2. Comparison of SIFs in large plate with central crack subjected to two symmetric pairs of equal, opposite and equidistant point forces.

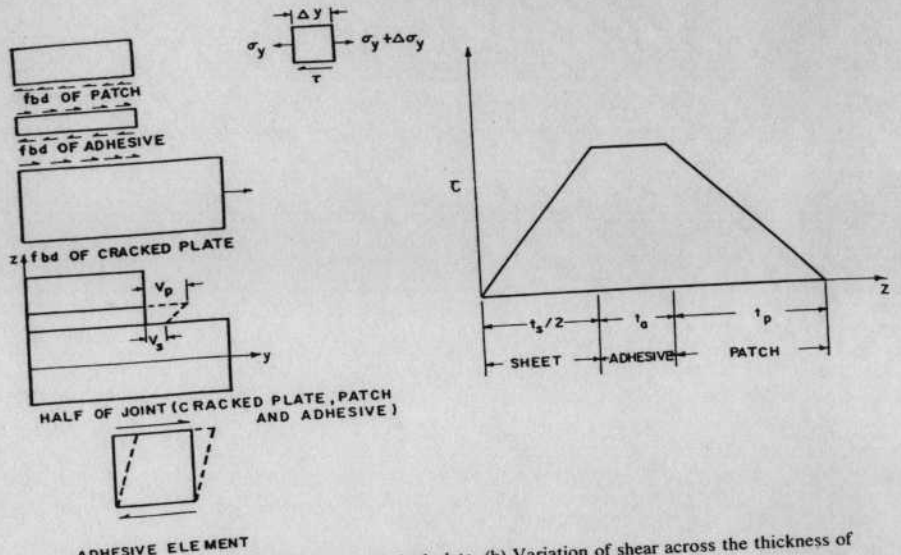

Fig. 3. (a) Schematic diagram of patched plate. (b) Variation of shear across the thickness of the patched plate.

for the adhesive shear stress,

$$\tau = \frac{G_a}{t_a}\frac{1}{g}(v_p - v_s) \tag{4}$$

where

$$g = 1 + \frac{1}{4}\frac{G_a/t_a}{G_s/t_s} + \frac{3}{8}\frac{G_a/t_a}{G_p/t_p}$$

As g is always greater than one, use of relation (4) is equivalent to increasing the shear flexibility of the adhesive layer. Consequently, the shear peaks are lowered and the variation is smoothened.

v_s is given as

$$v_s(x_0, y_0) = w\left[\int_0^t C_{sp}(x_0, y_0, y)\tau(x_0, y_0)\,dy_0\right]_{y=y_0} + C_{ss}(x_0, y_0)\sigma \tag{5}$$

where $C_{sp}(x_0, y_0, y)$ is the v displacement in the sheet at any point (x_0, y) due to unit point forces acting at $(\pm x_0, \pm y_0)$ points. $C_{ss}(x_0, y_0)$ is the v displacement in the sheet at any point (x_0, y_0) due to applied uniform stress, σ. C_{ss} from Ref. [12] is as follows:

$$C_{ss} = \frac{1}{E_s}\left[2\sqrt{(r_1 r_2)}\sin\frac{\theta_1 + \theta_2}{2} - y_0 - (1 + \nu)\frac{y_0}{\sqrt{(r_1 r_2)}} \times \left(x_0\cos\frac{\theta_1 + \theta_2}{2} + y_0\sin\frac{\theta_1 + \theta_2}{2} - \sqrt{(r_1 r_2)}\right)\right] \tag{6}$$

where

$$r_1 = [(x_0 - a)^2 + y_0^2]^{0.5};\quad r_2 = [(x_0 + a)^2 + y_0^2]^{0.5}$$
$$\theta_1 = \tan^{-1}(y_0/(x_0 - a));\quad \theta_2 = \tan^{-1}(y_0/(x_0 + a)).$$

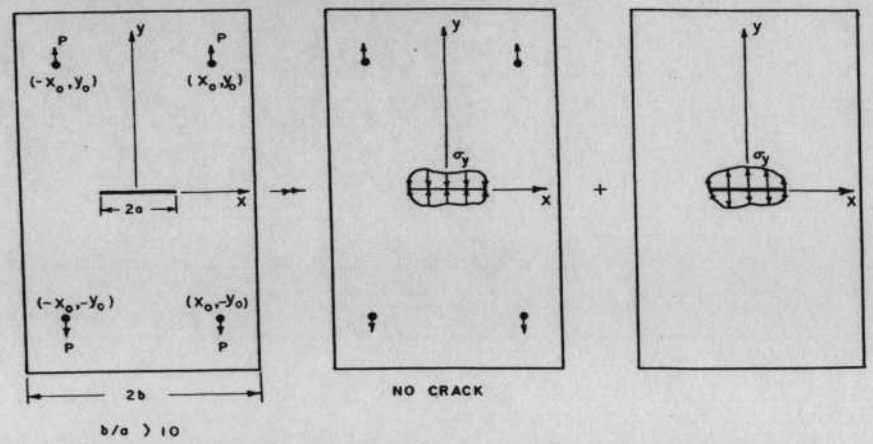

Fig. 4. (a) Large plate with central crack with a set of four point forces. (b) Large plate with a set of four point forces. (c) Large plate with central crack subjected to loading on crack faces.

2.1.1 *Determination of* C_{sp}. To determine C_{sp}, consider the displacement field in the cracked sheet due to four point forces as shown in Fig. 4. This is obtained by superposing the solutions of Figs. 4(b) and (c).

v_b, the y displacement at point (x_0, y) in an infinite plate due to unit forces at points $(\pm x_0, \pm y_0)$ (Fig. 4), is derived in Appendix B to yield

$$v_b(x_0, y_0, y) = \frac{(3 - \nu)(1 + \nu)}{8\pi E_s t_s}\ln\frac{\alpha_2^2(\alpha_2^2 + \alpha_3^2)}{\alpha_4^2(\alpha_3^2 + \alpha_4^2)} - \frac{(1 + \nu)^2}{\pi E_s t_s}\left[\frac{yy_0\alpha_3^2}{(\alpha_3^2 + \alpha_2^2)(\alpha_3^2 + \alpha_4^2)}\right]. \tag{7}$$

v_c, the y displacement at any point (x_0, y) in an infinite plate with a central crack due to distributed stress σ_y acting over the crack surfaces (fig. 4(b)) is obtained as follows: $\sigma_y(x_0, y_0, \xi, 0)$ due to unit forces at $(\pm x_0, \pm y_0)$ as derived in Appendix B is

$$\sigma_y(x_0, y_0, \xi, 0) = \frac{1 + \nu}{2\pi t_s}[f_5(x_0, y_0, \xi, 0) + f_6(x_0, y_0, \xi, 0)] \tag{8}$$

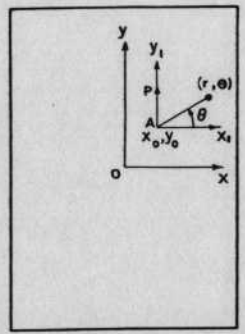

Fig. 5. Large plate with point force.

where

$$f_5 = \frac{3+\nu}{1+\nu}\frac{y_0}{(\xi - x_0)^2 + y_0^2} - \frac{2y_0(\xi - x_0)^2}{[(\xi - x_0)^2 + y_0^2]^2}$$

$$f_6 = \frac{3+\nu}{1+\nu}\frac{y_0}{(\xi + x_0)^2 + y_0^2} - \frac{2y_0(\xi + x_0)^2}{[(\xi + x_0)^2 + y_0^2]^2}.$$

The v displacement at point (x_0, y) due to pairs of unit forces acting on crack surfaces (Fig. 6) [13] is given as

$$v(x_0, y, \xi) = \frac{1}{\pi E_s t_s}(f_7 - f_8) \tag{9}$$

where

$$f_7 = \ln[C_3 + 2\sqrt{(C_3(C_1 + C_2))} + 2C_2] - \ln[C_3 - 2\sqrt{(C_3(C_1 + C_2))} + 2C_2]$$

$$f_8 = \frac{(1+\nu)\sqrt{C_3}}{C_2}\, y\left[\frac{C_4\sqrt{(C_2 - C_1)}x_0 - C_5 y\sqrt{(C_1 + C_2)}}{C_6^2 + 4x_0^2 y^2}\right]$$

$$C_1 = \tfrac{1}{2}(a^2 + y^2 - x_0^2); \quad C_2 = (C_1^2 + x_0^2 y^2)^{0.5}$$

$$C_3 = a^2 - \xi^2; \quad C_4 = x_0^2 + y^2 - \xi^2$$

$$C_5 = x_0^2 + y_0^2 + \xi^2; \quad C_6 = x_0^2 - y^2 - \xi^2.$$

The displacement v_c due to σ_y [as defined in eqn (8)] acting over the crack surfaces is obtained as

$$v_c = \frac{1+\nu}{2\pi^2 E_s t_s} I(x_0, t_0, y) \tag{10}$$

where

$$I(x_0, y_0, y) = \int_0^a (f_5 + f_6)(f_7 - f_8)\, d\xi$$

C_{sp} is obtained by adding relations (7) and (10) as follows

$$C_{sp} = \frac{(3-\nu)(1+\nu)}{8\pi E_s t_s}\left[-g_1 - \frac{8(1+\nu)}{(3-\nu)} g_2 + \frac{4}{\pi(3-\nu)} I\right] \tag{11}$$

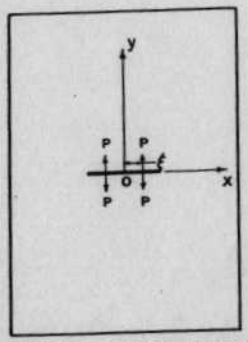

Fig. 6. Large plate with central crack with point forces acting on the crack faces.

where

$$g_1 = \ln\frac{\alpha_2^2(\alpha_2^2 + \alpha_3^2)}{\alpha_4^2(\alpha_3^2 + \alpha_4^2)}$$

$$g_2 = \frac{y y_0 \alpha_3^2}{(\alpha_3^2 + \alpha_2^2)(\alpha_3^2 + \alpha_4^2)}$$

g_1 is singular at $y = y_0$ and it is desirable to isolate the singular part. Thus

$$g_1 = 2\ln(y - y_0) + g_3 \tag{12}$$

where

$$g_3 = \ln\frac{\alpha_2^2 + \alpha_3^2}{\alpha_4^2(\alpha_3^2 + \alpha_4^2)}.$$

Using relations (11) and (12)

$$C_{sp} = -\frac{(3-\nu)(1+\nu)}{4\pi E_s t_s}\ln(y - y_0) + c_{sp_2} \tag{13}$$

where

$$C_{sp_2} = \frac{(3-\nu)(1+\nu)}{8\pi E_s t_s}\left[-g_3 - \frac{8(1+\nu)}{3-\nu} g_2 + \frac{4}{\pi(3-\nu)} I\right].$$

2.1.2 *Estimation of displacement v_p in the patch due to shear stress distribution.* From the patch equilibrium equation

$$\tau = t_p \sigma_{y,y} \tag{14}$$

where σ_y is the normal stress in the patch in the y-direction. Integrating eqn (14) and enforcing the zero normal stress condition at $y = l$ (free end)

$$\sigma_y = \frac{1}{t_p}\int_l^y \tau\, dy \tag{15}$$

Using stress–strain and strain–displacement relations

$$v_{p,y} = \frac{1}{E_p t_p}\int_0^l \tau\, dy. \tag{16}$$

Integrating eqn (16) and enforcing the symmetric (zero displacement) condition at $y = 0$

$$v_p = \frac{1}{E_p t_p}\int_0^y \int_y^l \tau\, dy^2. \tag{17}$$

2.1.3 *Governing equation in shear stress and its solution.* Using relations (4), (5) and (17), the following integral equation is obtained

$$\int_0^y \int_y^l \tau\, dy^2 - E_p t_p w\left[\int_0^l C_{sp}\tau\, dy\right] - \frac{E_p t_p t_a}{G_a}\cdot g\tau - E_p t_p \sigma C_{ss} = 0. \tag{18}$$

Equation (18) is solved by assuming a polynomial distribution for shear and employing a collocation technique.

Shear stress τ is assumed as follows

$$\tau = \sum_{j=1}^{n} A_j y^{j-1}. \tag{19}$$

Using relation (19) in eqn (18), the following relation results

$$\sum_{j=1}^{n} A_j f_j = \bar{G}\sigma C_{ss} \tag{20}$$

where

$$\bar{G} = \frac{1}{g}\frac{G_a}{t_a}$$

$$f_j = \frac{\bar{G}}{jE_pT_p}\left[\frac{y_0^{j+1}}{j+1} - l^j y_0\right] - y_0^{j-1} - w\bar{G}I_j(y_0)$$

$$I_j = \frac{(3-\nu)(1+\nu)}{4\pi E_s t_s} I_{j_1} + I_{j_2}$$

$$I_{j_1} = \int_0^l \ln(y - y_0) y_0^{j-1}\, dy_0$$

$$I_{j_2} = \int_0^l C_{sp_2} y_0^{j-1}\, dy_0.$$

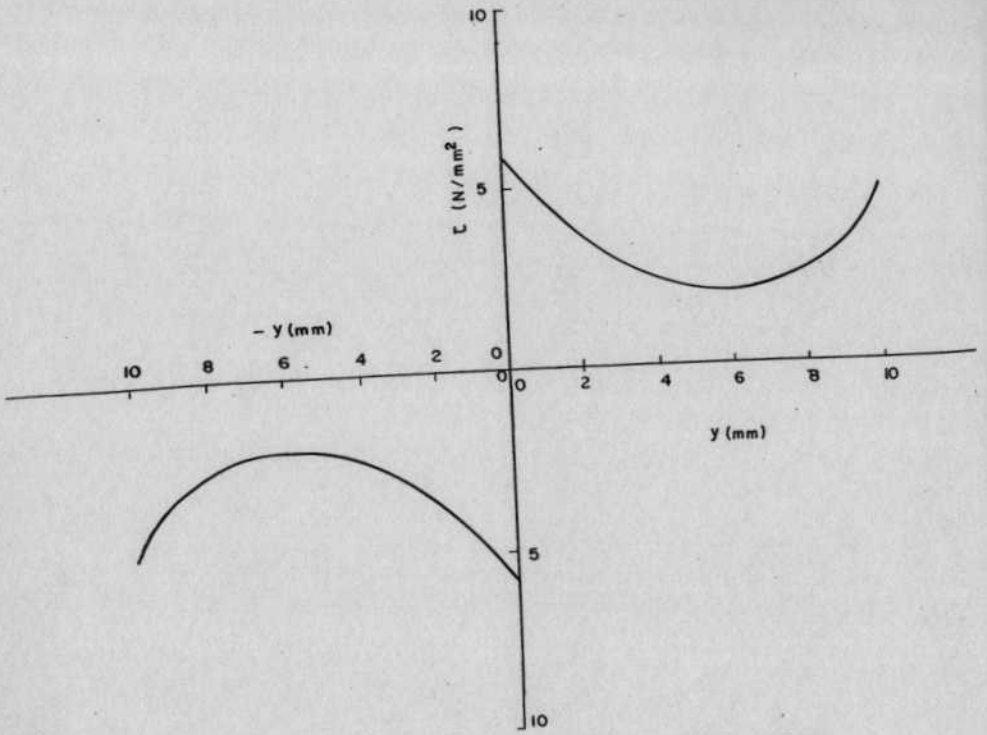

Fig. 7. Shear stress distribution along the patch length in photoelastic specimen.

I_{j_1} is singular at $y = y_0$; its numerical evaluation poses convergence problems. Hence I_{j_1} evaluated in closed form and is given as

$$I_{j_1} = -\sum_{r=0}^{j-1} \frac{(j-1)!}{r!(j-1-r)!}(-1)^r y^{j-1-r}\left[\frac{y^{r+1}\ln y}{r+1} - \frac{y^{r+1}}{(r+1)^2}\right]$$

$$-\sum_{r=0}^{j-1} \frac{(j-1)!}{r!(j-1-r)!} y^{j-1-r}\left[\frac{(l-y)^{r+1}(l-y)}{r+1} - \frac{(l-y)^{r+1}}{(r+1)^2}\right]$$

Collocating eqn (20) at n values of y_0,

$$[a]\{A\} = \{F\} \tag{2}$$

where

$$a_{ij} = f_j(y_i)$$

$$\{F\} = \bar{G}\sigma\{C_{ss}(y_1)C_{ss}(y_2) \ldots C_{ss}(y_n)\}^T$$

$$\{A\} = \{A_1A_2A_3 \ldots A_n\}^T.$$

The following collocation scheme is used

$$y_i = (i - 0.5)\frac{l}{(n-0.5)}, \qquad i = 1, 2, 3 \ldots n. \tag{2}$$

$\{A\}$ is obtained by solving eqn (21). Thus the shear stress distribution is determined from eq (19) and K from eqn (1).

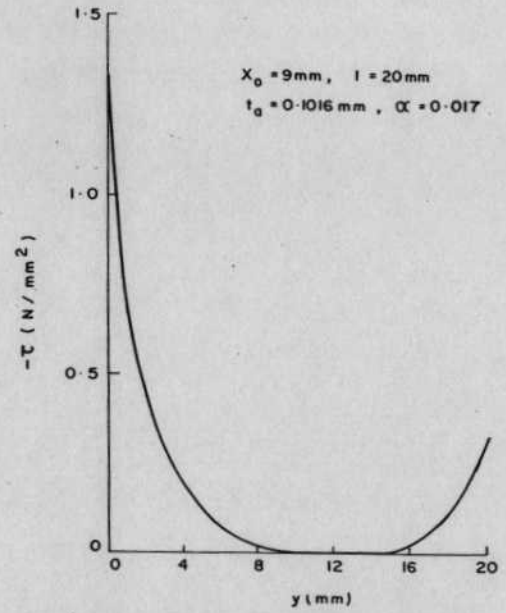

Fig. 8. Shear stress distribution in a typical patched plate.

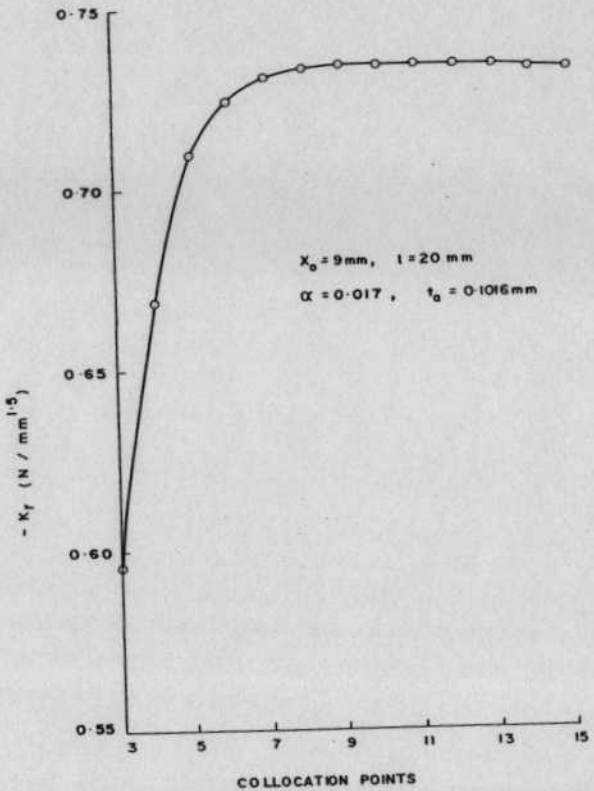

Fig. 9. Variation of K_r with collocation points in a typical patched plate.

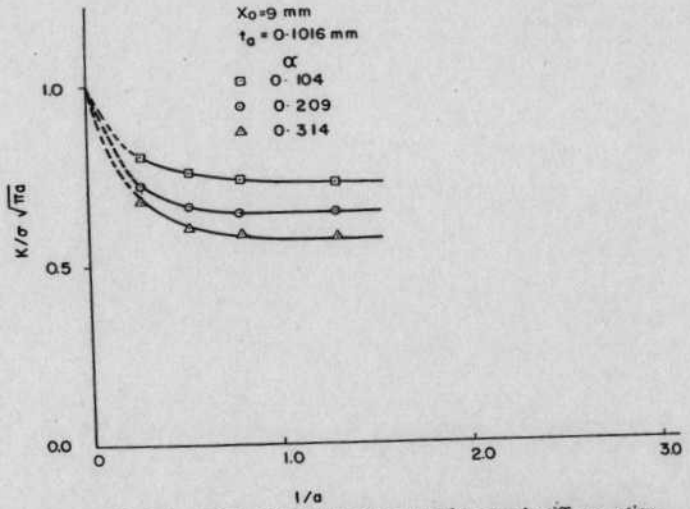

Fig. 10. Variation of SIF with patch length for various patch stiffness ratios.

3. RESULTS AND DISCUSSIONS

To validate the technique developed in this paper, let us consider a thin rectangular sheet of dimensions 75 × 340 × 2.96 mm, made of photoelastic material. The sheet contains a central crack of 25.5 mm length which is symmetrically patched on both sides by two photoelastic strips. The dimensions of the patch are: 20 × 2.5 × 1.71 mm. The 1.71 mm thick patches are bonded to the cracked sheet with a room temperature curing adhesive of 0.01 mm thickness. Young's moduli and Poisson's ratios of both patch and sheet are 3100 N mm^{-2} and 0.36, respectively. Shear modulus of sheet, patch and adhesive equals 1140 N mm^{-2}. The patch centre line is at a distance of 6.88 mm from the crack centre. The cracked sheet is subjected to a far field uniform stress of 3.61 N mm^{-2}. The shear stress distribution obtained is shown in Fig. 7. The theoretical value of SIF for this configuration is 15.22 N mm$^{-1.5}$ whereas the experimental value as obtained by employing the photoelastic technique [14], is 13.8 N mm$^{-1.5}$. The difference is within 10%.

Further numerical work is carried out for an aluminium alloy plate with carbon–epoxy patch with the following data:

E_s = 71,000 N mm^{-2}, ν = 0.3

G_s = 27,300 N mm^{-2}

E_p = 208,000 N mm^{-2}, G_p = 5000 N mm^{-2}

t_p = 0.127–0.762 mm

G_a = 965 N mm^{-2}, t_a = 0.1016 and 0.2032 mm

w = 2–10 mm, σ = 0.689 N mm^{-2}

x_0 = 5–19 mm, a = 19 mm

l = 5–30 mm.

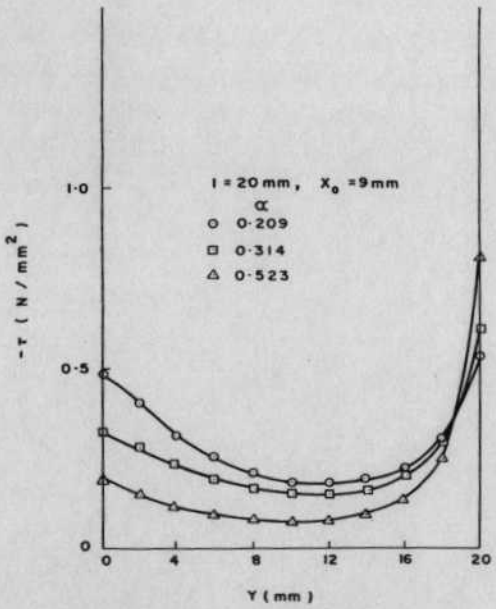

Fig. 11. Shear stress distribution in patched plate for various stiffness ratios.

Table 1. Adhesive shear distribution for various collocation points (CP)

CP	y/l					
	0	0.2	0.4	0.6	0.8	1.0
6	−1.169	−0.164	−0.019	−0.002	−0.027	−0.138
7	−1.267	−0.157	−0.020	−0.003	−0.023	−0.308
8	−1.304	−0.156	−0.019	−0.003	−0.024	−0.232
9	−1.327	−0.156	−0.019	−0.003	−0.024	−0.318
10	−1.331	−0.156	−0.020	−0.003	−0.024	−0.293
11	−1.329	−0.156	−0.020	−0.003	−0.024	−0.292

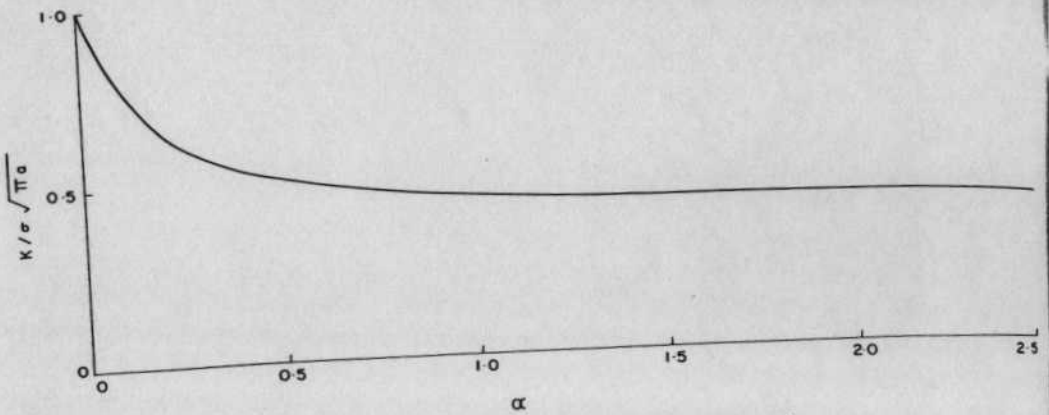

Fig. 12. SIF of patched plate for various values of stiffness ratios.

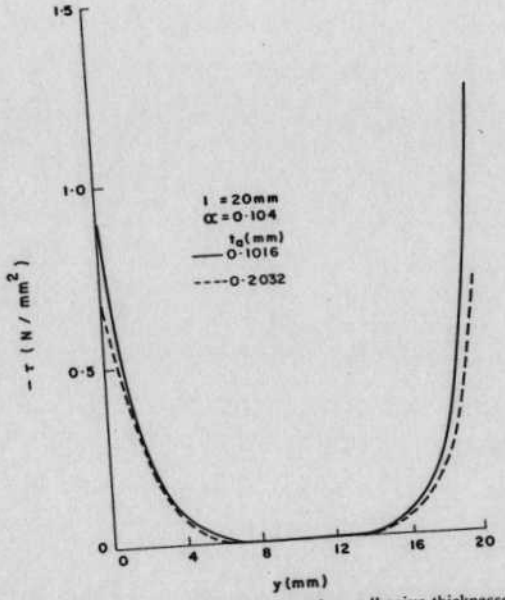

Fig. 13. Shear stress distribution for various adhesive thicknesses.

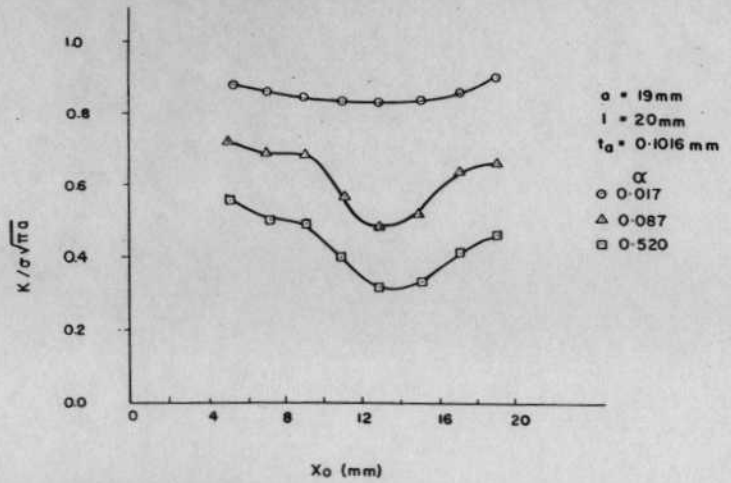

Fig. 14. Variation of SIF of patched plate with patch position for various stiffness ratios.

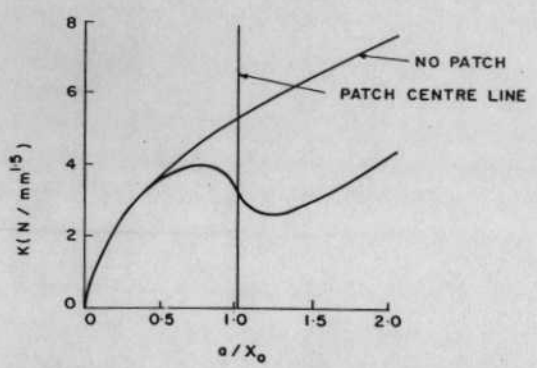

Fig. 15. Variation of SIF with crack length for fixed patch position.

In order to establish the optimum collocation points from the convergence view point, shea stresses and SIF(K_r) are estimated for a typical case with the number of collocation poin varying from 3 to 15. The convergence trend is good. The variation of values beyond nin collocation points is negligible. Table 1 and Fig. 8 show some details of shear stress distributio and convergence. Figure 9 shows the convergence of SIF(K_r) with the number of collocatio points.

Influence of patch length on SIF(K) is shown in Fig. 10. It is seen that the value of K virtual stabilizes at $l/a \simeq 1$. Hence, all further numerical work is carried out for a 40 mm patch leng ($l/a = 1.05$).

Figure 11 illustrates the effect of patch axial stiffness ratio, α, on shear stress distributio As expected, increase in patch stiffness results in increase of shear stress at the far end. Ho ever, the shear stress at the crack end is reduced by increasing patch stiffness. Figure 12 sho the effect of patch stiffness on SIF. Increasing stiffness ratio reduces SIF and it reaches asymptotic value for $\alpha = 2$. It is apparent that substantial reduction in SIF can be achiev with relatively small patch stiffnesses. Shear peaks at crack and far ends are naturally reduc with increasing the adhesive flexibility (t_a/G_a). This is shown in Fig. 13.

Figures 14 and 15 indicate the influence of patch position on SIF. There seems to be optimum patch position on the crack for which SIF is minimum. Figure 15 shows SIF vs cra

length for a fixed patch position. Such representation is useful to study crack growth in patched plates.

4. CONCLUSIONS

The main intention of the present work was to establish the methodology for continuum analysis of patched cracks. Although only line reinforcement is considered in the present work, the method can easily be extended to a two-dimensional patch by idealizing it as a series of line reinforcements. Such an idealization should be reasonably good because shear forces parallel to the crack are known to produce negligible changes in SIF. However, if a more accurate analysis is required, a two-dimensional model can be used for the patch. Such an analysis may be necessary to establish the actual benefits possible by covering the crack tip with a patch.

Although the problem of patched cracks has been treated in the past extensively through finite element methods, it appears that this is the first time that the problem is examined by a continuum approach. The advantages of this technique over finite element techniques are: (1) functional representation of shear stresses in the adhesive is feasible; (2) parametric study with less computational effort is possible.

From the parametric study carried out the following conclusions are drawn:

(1) There seems to be an optimum patch length beyond which there is no significant reduction in SIF.

(2) There seems to be an optimum position of patch with respect to crack for which the reduction in SIF is maximum.

Acknowledgements—Financial support for this work was provided by Aeronautics Research and Development Board. Thanks are due to Mr Jayant Sonavane for his computational assistance. Thanks are also due to Mr K. Purushothaman for his help in preparing the manuscript.

REFERENCES

[1] N. N., Damage tolerance and fatigue evaluation of structure FAA, 14 FCR Part 25, 571 (1977).
[2] N. N., Airplane damage tolerance requirements. MIL-Spec., 83444, USAF (1974).
[3] A. A. Baker and M. M. Hutchinson, Fibre composite reinforcement of cracked aircraft structure. Tech. Memo. ARL/Mat. 366, August (1976).
[4] A. A. Baker, A summary of work on application of advanced fibre composite at ARL Australia, *Composites* **9**(1), 11–16 (1978).
[5] R. Jones and R. J. Callinan, On the use of special crack tip elements in cracked elastic sheets. *Int. J. Fracture* **13**(1), 51–54 (1977).
[6] R. Jones and R. J. Callinan, Finite element analysis of patched cracks. *J. Str. Mech.* **7**(2), 107–130 (1979).
[7] R. Jones and R. J. Callinan, A design study on crack patching. *Fibre Sci. Tech.* **14**, 99–111 (1981).
[8] M. M. Ratwani, Analysis of cracked adhesively bonded laminated structures. *AIAA J.* **17**(9), 988–994 (1979).
[9] A. K. Rao, I. S. Raju and A. V. Krishna Murthy, A powerful hybrid method in finite element analysis. *Int. J. Num. Method Engng* **3**, 389–403 (1971).
[10] P. Tong, T. H. H. Pian and S. J. Lastry, A hybrid element approach to crack problems in plane elasticity. *Int. J. Num. Method Engng* **7**, 297–308 (1973).
[11] I. N. Sneddon and J. Tweed, The stress intensity factor for a Griffith crack in an elastic body in which body forces are acting. *Int. J. Fracture Mech.* **3**, 317–330 (1967).
[12] H. M. Westergaard, Bearing pressures and cracks. *J. Appl. Mech.* **16**(2), A49–A53 (1939).
[13] G. R. Irwin, Analysis of stresses and strains near the end of a crack traversing a plate. *Trans. Am. Soc. Mech. Engrs*, Series E, *J. Appl, Mech.* **24**(3), 361–364 (1957).
[14] A Subramanian and Ramesh Chandra, Stress intensity factors in plates with partially patched central crack, In *Communication with Experimental Mechanics*.
[15] C. T. Wang, *Applied Elasticity*. McGraw-Hill, New York (1953).

APPENDIX A
DETERMINATION OF SIF IN A LARGE PLATE WITH CENTRAL CRACK DUE TO TWO PAIRS OF POINT FORCES

DUE TO a concentrated load P at (x_0, y_0) (Fig. 5) the stress system is defined by the following Airy stress function

$$\psi = \frac{P}{8\pi t}\,\mathrm{Re}[i \ln(z - z_0)\{(3 - \nu)(z - z_0) + (1 + \nu)(\bar{z} - \bar{z}_0)\}]. \tag{A1}$$

$\sigma_y(\xi, 0)$ as obtained by using eqn (A1) is given as

$$\sigma_y(\xi, 0) = \frac{P}{8\pi t} \ln\left[\frac{5 + \nu}{\xi - z_0} - \frac{1 + \nu}{(\xi - z_0)^2}(\xi - \bar{z}_0)\right]. \tag{A2}$$

$\sigma_y(\xi_0)$ due to P at (x_0, y_0) and $-P$ at $(x_0, -y_0)$ is

$$\sigma_y(\xi, 0) = \frac{P}{\pi t} \ln\left(\frac{1}{\xi - z_0}\right) - \frac{1 + \nu}{2}\frac{P}{\pi t} y_0\,\mathrm{Re}\left(\frac{1}{(\xi - z_0)^2}\right). \tag{A3}$$

From Irwin's solution for the problem of cracked surfaces subjected to two equal and opposite point forces as shown in Fig. 6, SIF is given as

$$\mathrm{SIF} = \frac{2P}{t}\sqrt{\left(\frac{a}{\pi}\right)}\frac{1}{(a^2 - \xi^2)^{0.5}}. \tag{A4}$$

SIF due to $\sigma_y(\xi, 0)$ [as defined in eqn (A3)] is

$$\mathrm{SIF} = 2\sqrt{\left(\frac{a}{\pi}\right)}\int_{-a}^{a}\sigma_y(\xi, 0)\frac{1}{(a^2 - \xi^2)^{0.5}}\,d\xi. \tag{A5}$$

Using relations (A3) and (A5), SIF due to four unit point forces acting at $(\pm x_0, \pm y_0)$ is given as

$$\phi(x_0, y_0) = -\frac{2}{t}\sqrt{\left(\frac{a}{\pi}\right)}[\mathrm{Im}\{(z_0^2 - a^2)^{-0.5}\} + \left(\frac{1 + \nu}{2}\right)y_0\,\mathrm{Re}\{z_0(z_0^2 - a^2)^{-1.5}\}]. \tag{A6}$$

APPENDIX B
STRESS ANALYSIS OF INFINITE PLATE WITH POINT FORCES

STATE OF stress at a point due to load P at point A in infinite plate (Fig. 5) in polar coordinates as given in Ref. [15] is indicated as

$$\begin{aligned}\sigma_r &= -\frac{3 + \nu}{4\pi t}\frac{1}{r}P\sin\theta\\ \sigma_\theta &= \frac{1 - \nu}{4\pi t}\frac{1}{r}P\sin\theta\\ \sigma_{r\theta} &= -\frac{1 - \nu}{4\pi t}\frac{1}{r}P\cos\theta.\end{aligned} \tag{B1}$$

The above relations are rewritten in x_1y_1 coordinates as follows:

$$\begin{aligned}\sigma_{x_1} &= \frac{P}{4\pi t}\frac{\sin\theta}{r}[1 - \nu - 2(1 + \nu)\cos^2\theta]\\ \sigma_{y_1} &= -\frac{P}{4\pi t}\frac{\sin\theta}{r}[3 + \nu - 2(1 + \nu)\cos^2\theta]\\ \sigma_{x_1y_1} &= -\frac{P}{4\pi t}\frac{\cos\theta}{r}[1 - \nu + 2(1 + \nu)\sin^2\theta].\end{aligned} \tag{B2}$$

Relations (B2) are rewritten in xy coordinates as below

$$\begin{aligned}\sigma_x &= \frac{P}{4\pi t}\frac{y - y_0}{(x - x_0)^2 + (y - y_0)^2}\left[1 - \nu - 2(1 + \nu)\frac{(x - x_0)^2}{(x - x_0)^2 + (y - y_0)^2}\right]\\ \sigma_y &= -\frac{P}{4\pi t}\frac{y - y_0}{(x - x_0)^2 + (y - y_0)^2}\left[3 + \nu - 2(1 + \nu)\frac{(x - x_0)^2}{(x - x_0)^2 + (y - y_0)^2}\right]\\ \sigma_{xy} &= -\frac{P}{4\pi t}\frac{x - x_0}{(x - x_0)^2 + (y - y_0 0^2}\left[1 - \nu + 2(1 + \nu)\frac{(x - x_0)^2}{(x - x_0)^2 + (y - y_0)^2}\right].\end{aligned} \tag{B3}$$

State of stress at a point (x, y) due to four forces acting at points $(\pm x_0, \pm y_0)$ as shown in Fig. 4 is obtained from relations (B3). The expression for $\sigma_y(x, 0)$ is

$$\sigma_y(x, 0) = \frac{P(1 + \nu)}{2\pi t}\left[\frac{3 + \nu}{1 + \nu}\left\{\frac{y_0}{(x - x_0)^2 + y_0^2} + \frac{y_0}{(x + x_0)^2 + y_0^2}\right\} - 2y_0\left\{\frac{(x - x_0)^2}{((x - x_0)^2 + y_0^2)^2} + \frac{(x + x_0)^2}{((x + x_0)^2 + y_0^2)^2}\right\}\right]. \tag{B4}$$

Displacements are obtained as follows. Using stress–strain relation for the isotropic sheet

$$\epsilon_r = -\frac{(1+\nu)(3-\nu)}{4\pi Et}\frac{P\sin\theta}{r}$$
$$\epsilon_\theta = \frac{(1+\nu)^2}{4\pi Et}\frac{P\sin\theta}{r} \quad \text{(B5)}$$
$$\epsilon_{r\theta} = -\frac{1-\nu^2}{2\pi Et}\frac{P\cos\theta}{r}.$$

Using the strain-displacement relations

$$u(r,\theta) = -\frac{(3-\nu)(1+\nu)}{4\pi Et}P\sin\theta\ln r + A\cos\theta + B\sin\theta \quad \text{(B6)}$$
$$v(r,\theta) = -\frac{(1+\nu)^2}{4\pi Et}P\cos\theta - \frac{(3-\nu)(1+\nu)}{4\pi Et}\cos\theta\ln r - A\sin\theta + B\cos\theta + Cr$$

where A, B and C are arbitrary constants.
Displacements in x_1y_1 coordinates are

$$u(x_1,y_1) = \frac{(1+\nu)^2P}{4\pi Et}\sin\theta\cos\theta + A - Cr\sin\theta \quad \text{(B7)}$$
$$v(x_1,y_1) = -\frac{(3-\nu)(1+\nu)}{4\pi Et}P\ln r - \frac{(1+\nu)^2P}{4\pi Et}\cos^2\theta + B + Cr\cos\theta.$$

Displacements in xy coordinates are

$$u(x,y) = \frac{(1+\nu)^2P}{4\pi Et}\frac{(x-x_0)(y-y_0)}{(x-x_0)^2+(y-y_0)^2} + A - C(y-y_0)$$
$$v(x,y) = -\frac{(3-\nu)(1+\nu)}{8\pi Et}P\ln[(x-x_0)^2+(y-y_0)^2] - \frac{(1+\nu)^2P}{4\pi Et} \quad \text{(B8)}$$
$$\times\frac{(x-x_0)^2}{[(x-x_0)^2+(y-y_0)^2]} + B + C(x-x_0).$$

The displacements u and v due to a pair of point forces [P at (x_0, y_0) and $-P$ at $(x_0, -y_0)$] are

$$u = \frac{(1+\nu)^2P}{4\pi Et}\left[\frac{(x-x_0)(y-y_0)}{(x-x_0)^2+(y-y_0)^2} - \frac{(x-x_0)(y+y_0)}{(x-x_0)^2+(y+y_0)^2}\right] + 2A - 2Cy$$
$$v = -\frac{(3-\nu)(1+\nu)}{8\pi Et}P\ln\left[\frac{(x-x_0)^2+(y-y_0)^2}{(x-x_0)^2+(y+y_0)^2}\right] - \frac{(1+\nu)^2P}{4\pi Et} \quad \text{(B9)}$$
$$\times\left\{\frac{(x-x_0)^2}{(x-x_0)^2+(y-y_0)^2} - \frac{(x-x_0)^2}{(x-x_0)^2+(y+y_0)^2}\right\} + 2B + 2C(x-x_0).$$

Enforcing the boundary conditions $u(0, 0) = 0$, $v(x, 0) = 0$, A, B, and C are found to be zero.

Due to a pair of forces [P at $(-x_0, y_0)$ and $-P$ at $(-x_0, -y_0)$] u and v are obtained by substituting x_0 by $-x_0$ in relation (B9). Due to two pairs of forces [P at (x_0, y_0), $-P$ at $(x_0, -y_0)$, P at $(-x_0, y_0)$ and $-P$ at $(-x_0, -y_0)$] u and v are obtained as follows:

$$u = \frac{(1+\nu)^2P}{4\pi Et}\left[\frac{\alpha_1\alpha_2}{\alpha_1^2+\alpha_2^2} - \frac{\alpha_1\alpha_3}{\alpha_3^2+\alpha_1^2} + \frac{\alpha_3\alpha_2}{\alpha_3^2+\alpha_2^2} - \frac{\alpha_3\alpha_4}{\alpha_3^2+\alpha_4^2}\right]$$
$$v = -\frac{(3-\nu)(1+\nu)}{8\pi Et}P\ln\left[\frac{(\alpha_1^2+\alpha_2^2)(\alpha_3^2+\alpha_2^2)}{(\alpha_1^2+\alpha_4^2)(\alpha_3^2+\alpha_4^2)}\right] \quad \text{(B10)}$$
$$-\frac{(1+\nu)^2P}{\pi Et}\left[\frac{yy_0\alpha_1^2}{(\alpha_1^2+\alpha_2^2)(\alpha_1^2+\alpha_2^2)} + \frac{yy_0\alpha_3^2}{(\alpha_3^2+\alpha_2^2)(\alpha_3^2+\alpha_4^2)}\right]$$

where

$$\alpha_1 = x - x_0, \quad \alpha_2 = y - y_0$$
$$\alpha_3 = x + x_0, \quad \alpha_4 = y + y_0.$$

v at $x = x_0$ is obtained from the above relation as follows:

$$v = -\frac{(3-\nu)(1+\nu)}{8\pi Et}P\ln\left[\frac{\alpha_2^2(\alpha_3^2+\alpha_1^2)}{\alpha_4^2(\alpha_3^2+\alpha_4^2)}\right] - \frac{(1+\nu)^2P}{\pi Et}\frac{yy_0\alpha_3^2}{(\alpha_3^2+\alpha_2^2)(\alpha_3^2+\alpha_4^2)}. \quad \text{(B11)}$$

Engineering Fracture Mechanics Vol. 21, No. 3, pp. 495–501, 1985
Printed in the U.S.A.

0013-7944/85 $3.00 + .00

AN APPROXIMATE ELASTOPLASTIC ANALYSIS OF THE EFFECT OF PLANE STRAIN AT THE SURFACE OF A NOTCH

A. E. GEMMA
United Technologies Corp., Commercial Products Division, Pratt & Whitney Aircraft Group, 400 Main Street (MS 165-14), East Hartford, CT 06108, U.S.A.

Abstract—An approximate elastoplastic analysis of a notch in plane strain is developed using an extended Neuber approach. The multiaxial stress/strain state at the notch surface is dependent upon a parameter which is readily obtained from the numerical solution of a transcendental equation for each level of the net section stress. Excellent agreement with the results of a finite element analysis of a double-edge-notched specimen was obtained.

NOTATION

e_{ij}	net section strain tensor
E	elastic modulus
K_t	elastic stress concentration factor; eqn (6)
K_σ, K_ϵ	parameters in Neuber relationship; eqn (6)
n	parameter in Ramberg–Osgood relationship
N_{ij}	net section stress tensor
S_{ij}	stress deviator
δ_{ij}	Kronecker delta
ϵ_{ij}^e	elastic strain tensor
ϵ_{ij}^p	plastic strain tensor
ϵ_e^p	effective strain
λ	constraint parameter
ν	Poisson ratio
σ_{ij}	stress tensor
σ_0	parameter in Ramberg–Osgood relationship
σ_e	effective stress
Φ	see eqn (18)

INTRODUCTION

THE FATIGUE life of a structure is largely determined by the presence of localized regions of stress/strain concentration. The concentrations may be due to pre-existing material defects, e.g. inclusions, cracked carbides, etc., or may be the result of configurations required by design considerations, e.g. holes, grooves, slots, etc. Defects introduced by the fabrication process such as hole drilling methods are also sources of concentrations.

The surface of a notch in a thick section is subject to a biaxial stress state; the constraint produces a higher maximum stress than would be the case for a similar notch in a thin sheet. Biaxial stress conditions have also been found to have a significant effect on low cycle fatigue life (LCF) [1]. In a recent study of surface crack initiation in thick plate specimens with a center hole machined normal to the plate surface, the constraint due to the thickness was found to be important. Careful fractographic examination revealed that the crack initiation site was at the surface of the hole near the mid-thickness region, where the degree of constraint is greatest and the corresponding biaxiality produces a higher stress than for a thin plate [2]. Prantl in an experimental study of the constraint effects in deep notches arrived at similar conclusions [3].

The biaxial elastoplastic stress/strain state at a notch surface can be estimated by a plane strain analysis. Although finite element or boundary integral methods can be used to obtain solutions to these problems, they are usually expensive and time-consuming and a simpler approach may be desirable. Several graphical and *ad-hoc* methods have been proposed to account for the multiaxial state of stress at a notch surface [4–7]. Since the underlying assumptions are not made explicit, these methods are difficult to evaluate. For this reason, pains were taken to make the following approximate analysis both clear and self-contained.